e-ISSN 2083–4640
ISSN 1507–1367

RESEARCH PAPER

Reports of Practical Oncology and Radiotherapy
2024, Volume 29, Number 4, pages: 478–487
DOI: 10.5603/rpor.102129
Submitted: 19.05.2024
Accepted: 16.08.2024

Heterogeneity in biological response of MDA-MB-231 cells after proton irradiation along different parts of the depth-dose curve: before, within, and behind the Bragg peak

Marika Musielak[1–3], Kinga Graczyk[4, 5], Małgorzata Liszka[5], Eleftherios Papalanis[6], Wiktoria Suchorska[1, 3], Tomasz Piotrowski[1, 4], Bo Stenerlöw[6], Julian Malicki[1, 4]

[1]Department of Electroradiology, Poznan University of Medical Sciences, Poznan, Poland
[2]Doctoral School, Poznan University of Medical Sciences, Poznan, Poland
[3]Radiobiology Laboratory, Department of Medical Physics, Greater Poland Cancer Centre, Poznan, Poland
[4]Department of Medical Physics, Greater Poland Cancer Centre, Poznan, Poland
[5]The Skandion Clinic, Uppsala, Sweden
[6]Department of Immunology, Genetics and Pathology, Rudbeck Laboratory, Uppsala University, Uppsala, Sweden

ABSTRACT

Background: Proton therapy has garnered attention as an advanced radiation treatment modality for breast cancer due to its ability to deliver highly precise doses to the target area while minimizing exposure to surrounding healthy tissues. The aim was to detect potential variations in radiobiological response along different parts of the proton depth-dose curve.

Materials and methods: MDA-MB-231 cells were specifically irradiated before, within, and beyond the Bragg peak with a 5 Gy dose, with photons used as a reference. The radiobiological response was evaluated using clonogenic assays, relative γH2AX levels, and quantitative polymerase chain reaction (qPCR) analysis of DNA damage response genes.

Results: A trend of increasing magnitude in radiobiological response was observed with increasing depth of cell irradiation, accompanied by a decrease in survival fraction. Furthermore, differences were noted, particularly in γH2AX levels along the Bragg peak, with higher values of DNA double-strand breaks (DNA DSB) observed at the end of the depth-dose curve.

Conclusions: These findings suggest that despite administering a consistent proton dose to the target area, there can be a range of different biological reactions, which might have significant indications for clinical procedures.

Key words: radiotherapy; protons; oncology; breast cancer; depth-dose curve

Rep Pract Oncol Radiother 2024;29(4):478–487

Introduction

Due to precise irradiation (IRR) techniques, high conformal dosage in the target volume and remarkably limited doses in the surrounding organs, proton therapy is becoming a promising method of treating hard-to-reach tumors [1]. Moreover, the distinctive radiobiological properties of proton beams offer a beneficial treatment option for radioresistant subtypes of breast cancer (BC). This

Address for correspondence: Marika Musielak, Department of Electroradiology, Poznan University of Medical Sciences, Poznan, Poland; e-mail: marikamusielak@gmail.com

alternative could potentially be more cost-effective than photon radiotherapy (RT), particularly for patients with increased cardiovascular risks [2]. The characteristic feature of proton therapy is a depth-dose curve called a Bragg peak [3]. Compared to the conventional photon RT, proton therapy includes protons, which interact differently with cancer tissue [4]. It is associated with a low entering dose, deposition of the maximum energy (Bragg peak) in the target and a minimal dose behind the irradiated target [5]. Because of the closely located organs during BC irradiation, named organs at risk (OAR), RT planning is still challenging to achieve the highest possible effectiveness [6]. Standard proton RT uses a spread-out Brag peak (SOBP) for which dose and biological response can be measured. Still, it is averaged and comes from mixed processes responsible for ionization through different interactions of protons, scattered electrons and scattered photons with BC cells [7].

Different physical processes are responsible for energy transfer when protons travel through the tissues. These interactions cause specific shape of the depth-dose with a peak (Bragg) at the energy-dependent depth. Due to different nature of these interactions the biological response before, at the peak and after the peak can differ. The distinctive Bragg peak is linked to protons' enhanced deceleration as they traverse a medium, resulting in a decrease in their speed. Protons interact with matter through three primary mechanisms: inelastic nuclear reactions with the medium's nuclei, causing scattering [8, 9]. Accuracy, end-of-range effects (range inconsistency), changes in enhanced linear energy transfer (LET), and relative biological effectiveness (RBE) at the distal edge of proton beams, which may increase toxicity, are still technical obstacles for clinicians [10, 11]. Therefore, clinical evidence still needs to be stronger, as does the knowledge of physical effects leading to a dose and its biological effectiveness along different parts of the depth-dose curve, particularly before, within and behind the Bragg peak [12].

The methodology of proton therapy includes the superpositions of multiple beams with different energy levels. The absorption of energy before, within, and after the Bragg peak across the depth-dose curve constitutes the dosage delivered to the target area. Consequently, the extent and nature of biological effects induced by proton beam radiation remain uncertain. This study aimed to assess any differences in the biological response of BC cells to radiation from proton beams across the depth-dose curve.

Materials and methods

Irradiation conditions and dosimetric verification

The MDA-MB-231 cells were placed and irradiated with photon and proton beams in a water phantom at five locations along the percentage depth dose (PDD) curve. The MP1 water tank (PTW Freiburg, Germany) is a small phantom (external dimensions: 320 mm × 370 mm) with a precise vertical moving mechanism (range: 254 mm and positioning accuracy: 0.1 mm), designed for depth dose measurement to determine beam qualities. Its design meets the criteria of the American Association of Physicists in Medicine (AAPM) TG 51 [13] and International Atomic Energy Agency (IAEA) TRS 398 [14] reports for reference conditions. The experiment was carried out in two medical facilities: the Greater Poland Cancer Centre, where a linear accelerator generating a photon beam with an effective acceleration potential of 6 MV was used, and at the Skandion Clinic, where an isochronous cyclotron generating a proton beam in the range from 60 MeV to 226 MeV was used.

Based on the PDD for 6 MV FF (with flattering filter) photon beam and 150 MeV proton beam, measured with Semiflex 3D cylindrical ionization chamber (PTW) and Ross plane-parallel ionization chamber (PTW), attached to the moving mechanism with a dedicated handle, the optimal location of cell culture bottles, experimental setup and beam parameters for the irradiation of biological material with a homogenous (field size: 10 × 10 cm) 5 Gy dose at each point, was determined (Fig. 2). Selected positions (i.e. the red dots marked in Fig. 1) correspond to characteristic regions in the percentage depth dose curve. For photon beam: P1, P2 — dose build-up region, P3 — maximum dose, P4, P5 — dose fall-off region, and for proton beam: P1 — plateau, P2 — dose build-up region, P3 — maximum dose (Bragg peak), P4, P5 — dose fall-off region.

A three-dimensional printer (Prusa Research, Prague, Czech Republic) was used to print a purpose-built holder (Fig. 2B). This holder was then

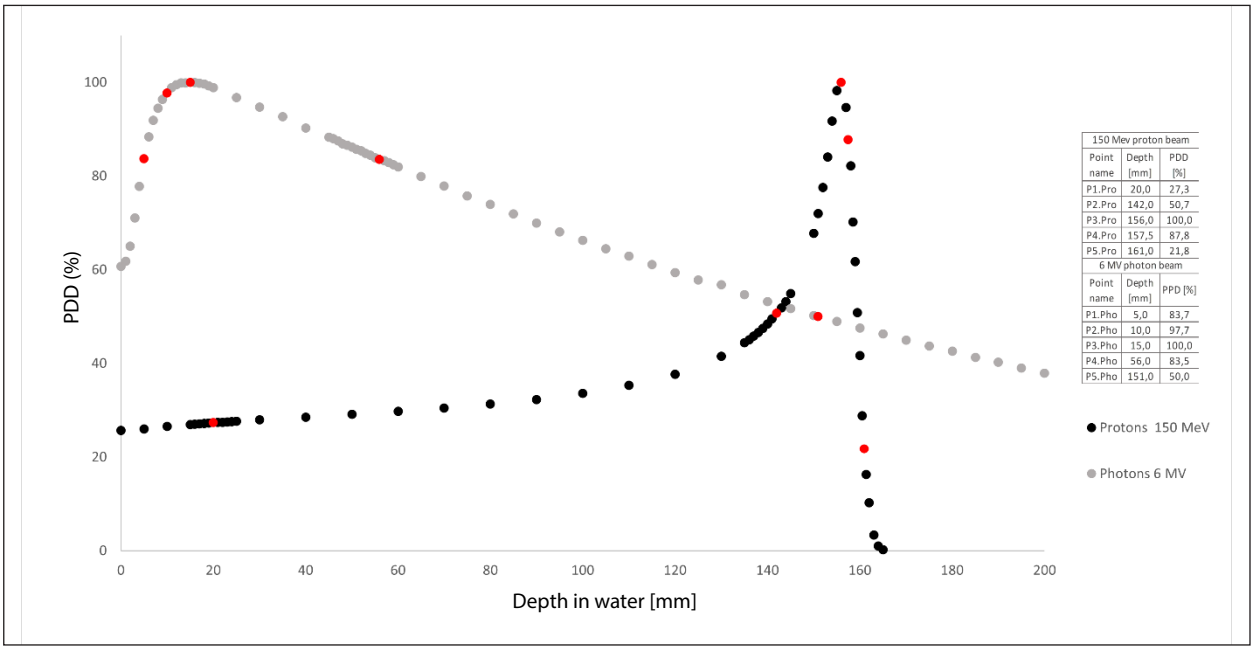

Figure 1. Percentage depth dose for 150 MeV proton beam (black) and 6 MV photon beam (grey). MDA-MB-231 cells were irradiated in five different locations along the depth-dose curve. Each point was noted with a red dot. The percentage depth dose (PDD) measurements were performed using an MP1 water phantom, Markus Advanced (proton beam) and Semiflex 3D (photon beam). Px.Pro — cells position number x for proton beam irradiation; Px.Pho — cells position number x for photon beam irradiation

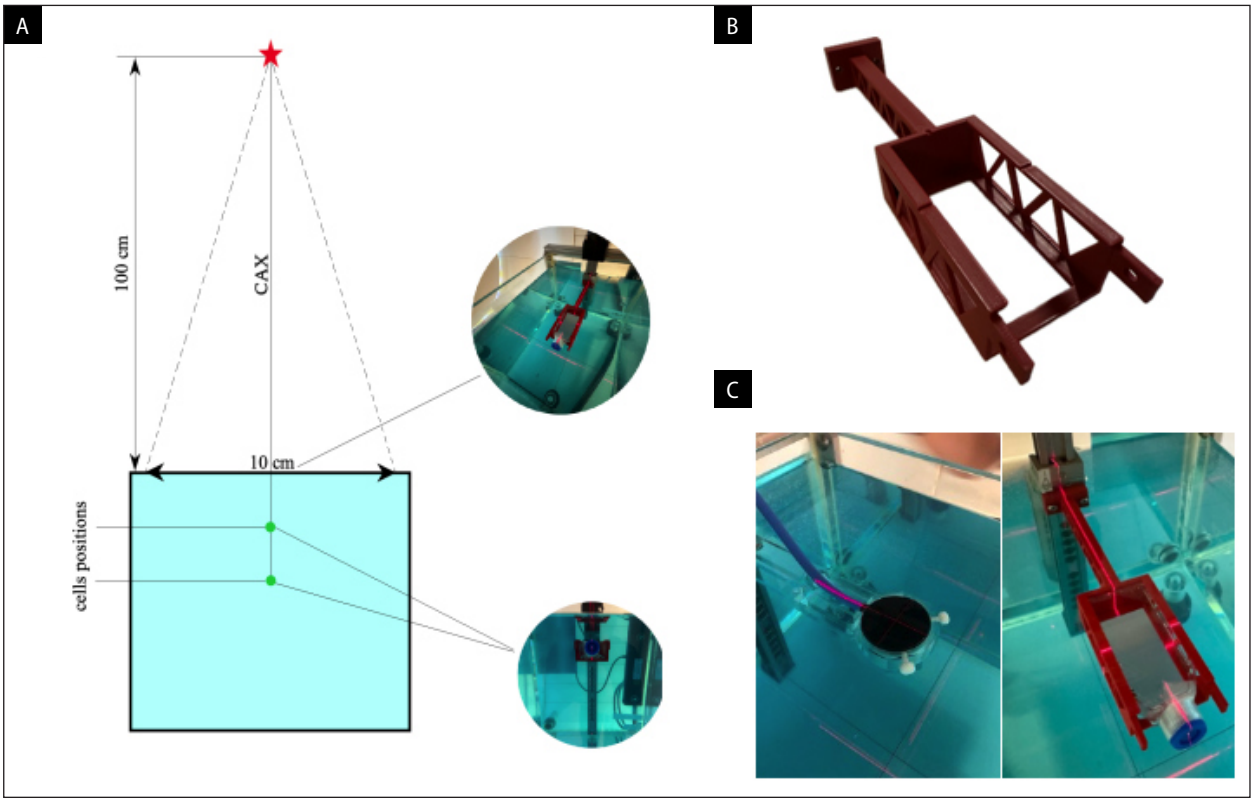

Figure 2. Individual elements used to conduct an experiment involving biological material — the MDA-MB-231 cells. **A.** Scheme of the experimental setup consisting of a water phantom with precise vertical moving mechanism allowing to change the depth of the measurement chamber and the bottle with cells to the appropriate position; **B.** Dedicated T-25 bottle holder, made using 3D printing technology; **C.** Mounting to dedicated holders in corresponding positions, two components used to conduct the experiment in a water phantom — measuring chamber and T-25 bottle

installed in the water phantom in place of the original measuring holder with ionization chamber (Fig. 2A) so that the position of the active volume of the measuring chamber corresponds to the center of the bottle wall on which the cells were sown (Fig. 2C). During planning the beam parameters, differences in water equivalence thickness (WET) for the bottle wall and individual ionization chambers were considered.

Dosimetry pre-verification was performed, using GAFChromic EBT4 films (Ashland Inc., Wilmington, Delaware, USA), which allows dose measurement in the range of 0.2 Gy to 10 Gy with high resolution [15]. The films were attached to one of the walls of the bottle (Fig. 2C), where the cells will ultimately be located.

All activities using radiochromic films were subordinated to the recommendations described in the AAPM TG 235 report. The EBT4 films were calibrated in solid water phantom against known doses ranging from 0.5 to 7 Gy. After radiation exposure, the films were placed in a dedicated envelope for 24 hours to allow the post-irradiation growth to stabilize.

The films were scanned in the same orientation with a glass plate on top, using the Epson Perfection 10000 XL scanner (Seiko Epson Corporation, Japan) with the following parameters: no colour correction, transmission mode, portrait orientation, 48-bit Red–Green–Blue (RGB). The scan resolution was 72 dpi for calibration and measurements. Scans were then (analyzed using Film QA Pro (Ashland Inc., Wilmington, Delaware, USA).

Cell culture

In the study, the MDA-MB-231 BC cell line (ATCC) was used. For MDA-MB-231 cell culture, DMEM (Biowest, France) supplemented with 10% of fetal bovine serum (FBS) (Biowest, France), and the 1% of penicillin/streptomycin complex (P/S) (Merck Millipore Corporation, Germany) was applied. Cells were cultured at 37°C in a standard atmosphere enriched with 5% CO_2 and saturated with a water vapor incubator (Binder, Germany). All experiments were performed under aseptic conditions in a laminar flow hood.

Cell irradiation

MDA-MB-231 cells were seeded on T-25 bottles (Thermo Fisher Scientific Inc., Waltham, Massachusetts, USA, catalog no. # 63371). After 24 h, bottles were filled to capacity with PBS removing air bubbles to maintain the homogenous irradiation dose. Irradiation was performed in the water phantom. BC cells were irradiated with the 5 Gy dose on 5 chosen localization along different part of depth-dose curve. The control group was prepared in the same way as irradiated cells, but did not received irradiation.

Clonogenic assay

Following irradiation, cells were harvested and separated to prepare the clonogenic assays. After 7 days of incubation, cells were washed with PBS and fixed using denatured ethanol. Next, cells were stained with Coomassie Blue solution (Merck Millipore Corporation, Germany) and incubated for 20 min. After staining, plates were washed with warm water and left to dry overnight. Clonogenic tests were photographed applying the ChemiDoc Touch Bio-Rad system (Hercules, USA). Automatic colony counting was performed using the Gene Tools Syngene program.

γH2AX by flow cytometry

After irradiation cells were immediately transported to the laboratory. Post 1 h, cells were harvested, washed using PBS and fixed with the Fixation/Permeabilization Kit (BD Biosciences, NJ, USA). The 3.5 µL anti-γH2AX antibody (Becton Dickinson, USA) was applied for cell staining in the final volume of 20 µL. Samples were incubated for 30 min at 4°C. Finally, the volume of 180 µL PBS was added to each samples to cytometric analysis. For flow cytometry analysis, the Cytoflex Beckman Coulter cytometer (Beckman Coulter Life Sciences, ID, USA) was used. Analysis of the obtained results was performed using FlowJo v10 (FlowJo LLC, USA). Immunofluorescence of stained cells was imaged using Olympus IX83 Inverted Fluorescence Microscope.

Quantitative polymerase chain reaction (qPCR) analysis

For quantitative polymerase chain reaction (qPCR) analysis, RNA was isolated applying Direct-zol RNA MiniPrep (Zymoresearch, Irvine, CA, USA). After 24 h, cells were collected using TRI reagent (Sigma-Aldrich, St. Louis, MO, USA). Each cell sample included 1×10^6

cells. After obtaining 1 µg of total RNA, the reverse transcription was completed using iScript kit (Bio-Rad, Hercules, CA, USA). The cDNA was prepared in a total volume of 20 µl and diluted 5 times. Next, the expression of genes was analyzed using RT-qPCR. The RealTime ready assays were used (Roche Diagnostics, Germany): GAPHD assay ID: 05190541001, MSH2 assay ID: 11082, PRDKC assay ID: 147005, APEX1 assay ID: 137234, XRCC4 assay ID: 114754, XRCC1 assay ID: 148350, MSH6 assay ID: 145606, RAD51 assay ID: 101531. The reference gene was human GAPDH to determine relative expression. The PCR reaction was conducted in CFX96 Touch Real-Time Detection System (Bio-Rad Hercules, CA, USA) using volume of 10 µl.

Statistical analysis

PQStat Software v.1.8.2 was used for the statistical analysis. The Shapiro-Wilk test was conducted to determine the normality of the obtained results. The one-way ANOVA was used for comparing multiple groups. Tukey's post hoc test was amplified to analyze the diversity for a complex system (more than two groups) and multiple comparison procedures. If Levene's test showed that the variances were not equal across the groups, the unequal variance t-Test (Welch's t-Test) was applied. For comparing two independent groups, the t-student test was applied. For the correlation analysis the Pearson correlation was used. The p-value = 0.05 was administered to indicate whether the data were significant. The setting of the p-value was $*p < 0.05$, $**p < 0.01$, $***p < 0.001$.

Results

Dosimetric verification

The dose delivered to the cells was validated using EBT4 GAFchromic films for proton and photon beam irradiation. Separate calibration curves were prepared for both beams against known doses in the same range. A dose of 5 Gy was planned for each of the experimental points. The obtained results of dose verification measurements are shown in Figure 3. Three measurement series were carried out for each point. The volume of interest of the films included in the analysis was 5 cm × 3 cm. For the proton beam, the best agreement between the planned (5 Gy) and measured doses was obtained for P1 located in the plateau area, where the measured dose was 5.006 ± 0.027 Gy. For photons an agreement was observed for P2 - the measured dose was 5.007 ± 0.025 Gy. The largest differences between these doses (planned *vs* measured) were noted, respectively: for protons in P3, where the measured dose was 5.101 ± 0.046 Gy and for photons in P5 — the measured dose was 4.877 ± 0.063 Gy. The relative difference did not exceed 2.5% at any point, which proves high compliance between the measured and planned doses.

MDA-MB-231 cell surviving fraction after proton and photon IRR

To assess heterogeneity in biological response along the depth-dose curve, BC cells were irradiated with a proton beam in 5 locations along different parts of the Bragg curve (P1–P5). A decreasing surviving fraction (SF) trend was observed in cells ir-

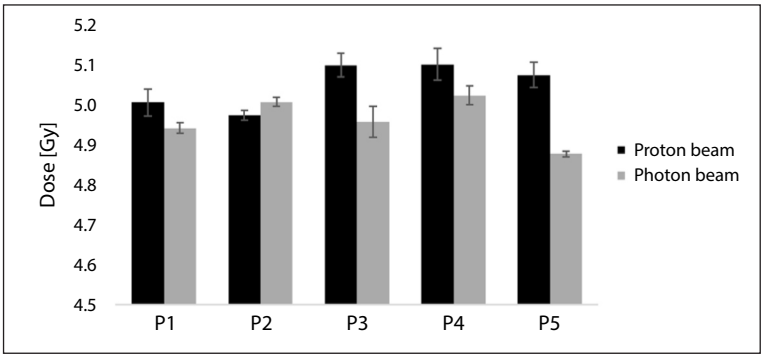

Figure 3. The graph shows the results of dosimetric pre-verification of the planned experiment involving biological material for proton (black bars) and photon beam (gray bars). The dose was measured using EBT4 radiochromic films, each measurement was performed three times for each point. The error bars represent standard deviation (SD). IRR — irradiation

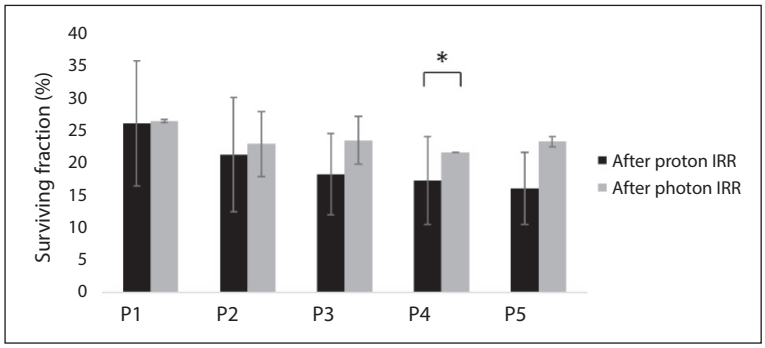

Figure 4. The surviving fraction (SF) of MDA-MB-231 cells after proton and photon irradiation (IRR). Cells were irradiated in 5 different locations along different part of depth-dose curve (P1–P5). The irradiation dose in each point was 5 Gy. The setting of the p-value was *p < 0.05. The error bars represent standard deviation (SD)

radiated with proton IRR (Fig. 4). In P1, SF reached 26%, while in the deepest P5, the SF was 16%. With increasing depth at which cells were irradiated, SF was reduced. In contrast, BC cells indicated 26% and 23% of SF value after photon IRR in P1 and P5, respectively. Considering variable effects between photon and proton IRR, a statistically significant difference was observed for P4. The proton IRR caused significantly lower SF in BC cells than the photon IRR ($p = 0.024722$).

γH2AX levels in MDA-MB-231 cells after IRR

Following proton and photon irradiation, cells were analyzed to investigate the γH2AX levels using flow cytometry (Fig. 5). The increased val-

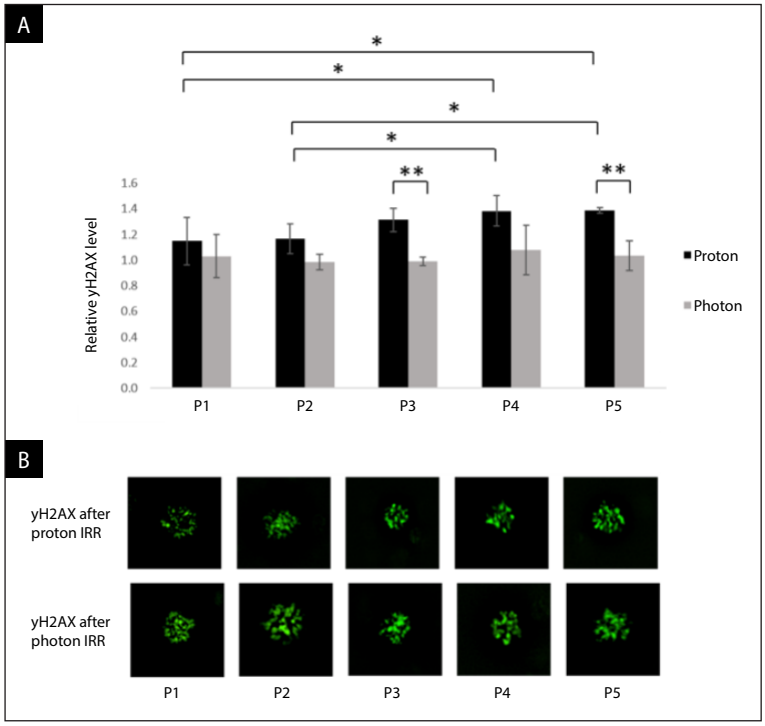

Figure 5. γH2AX level generated in MDA-MB-231 cells after 1h post proton and photon irradiation (IRR). Cells were irradiated in 5 different locations along different part of depth-dose curve (P1–P5). **A.** The relative γH2AX level was analyzed using flow cytometry; **B.** Same cells used for flow cytometry analysis were pictured to compare the γH2AX immunofluorescence visually. Immunofluorescence of stained cells were pictured using Olympus IX83 Inverted Fluorescence Microscope (magnification X40). The setting of the p-value was *p < 0.05, **p < 0.01. The error bars represent standard deviation (SD)

ues of γH2AX were observed comparing different irradiation points after proton IRR (Fig. 5A). The depth-dependent pattern in rising γH2AX levels was noticed, with increasing depth at which cells were irradiated, the γH2AX level was higher. There were statistically significant differences in DNA double strand-breaks (DNA DSB) levels between P1 *vs*. P4 and P5 locations (P1 *vs*. P4 p = 0.034513; P1 *vs*. P5 p = 0.032537). Similarly, statistically significant differences were noted with P2 (P2 *vs*. P4 p = 0.049089; P2 *vs*. P5 p = 0.032537). The γH2AX value in P3 location did not differ significantly compared to other locations. There was no difference in DNA DSB level between various irradiation points in the photon beam. Interestingly, comparing the effects of proton and photon IRR in one localization point, the differences were spotted in the P3 and P5 points. The P3 position was where the dose reaches 100% in RT. Considering various kinds of IRR, in each of the abovementioned points, the γH2AX levels were higher after proton IRR. Statistically, the p-values of proton and photon beam comparisons in one location were p = 0.004386 in P3 and p = 0.007281 in P5. The statistical correlation between SF and γH2AX levels indicated that as the location changes along the Bragg peak, there is a relationship of increasing γH2AX levels with decreasing SF. Each analyzed point corresponded to the irradiation location. The Pearson R^2 parameter was 0.38, while the p-value was 0.006.

Moreover, immunofluorescence microscopy imaged the same cells as those used for flow cytometry γH2AX analysis (Fig. 5B). A higher intensity of γH2AX after proton IRR was observed. The γH2AX foci were visible after both types of IRR, but the size of each foci was incomparable. Cells were not attached to plates, thus the foci measurements could not be performed.

The gene expression after IRR

The qPCR analysis was executed for gene expression investigation (Fig. 6). MDA-MB-231 cells were collected after 24 h post-IRR to assess whether genes associated with radiobiological responses differ between various IRR locations along the depth-dose curve. The expression of the following genes was analyzed — *MSH2*, *PRDKC*, *APEX1*, *XRCC4*, *MSH6*, *XRCC1* and *RAD51*. The aim was to observe potential differences between chosen IRR locations P1–P5. No statistical difference was observed in the gene expression between the cells that were irradiated at various depths along the Bragg peak. The homogenous response in expressed genes was observed after proton ir-

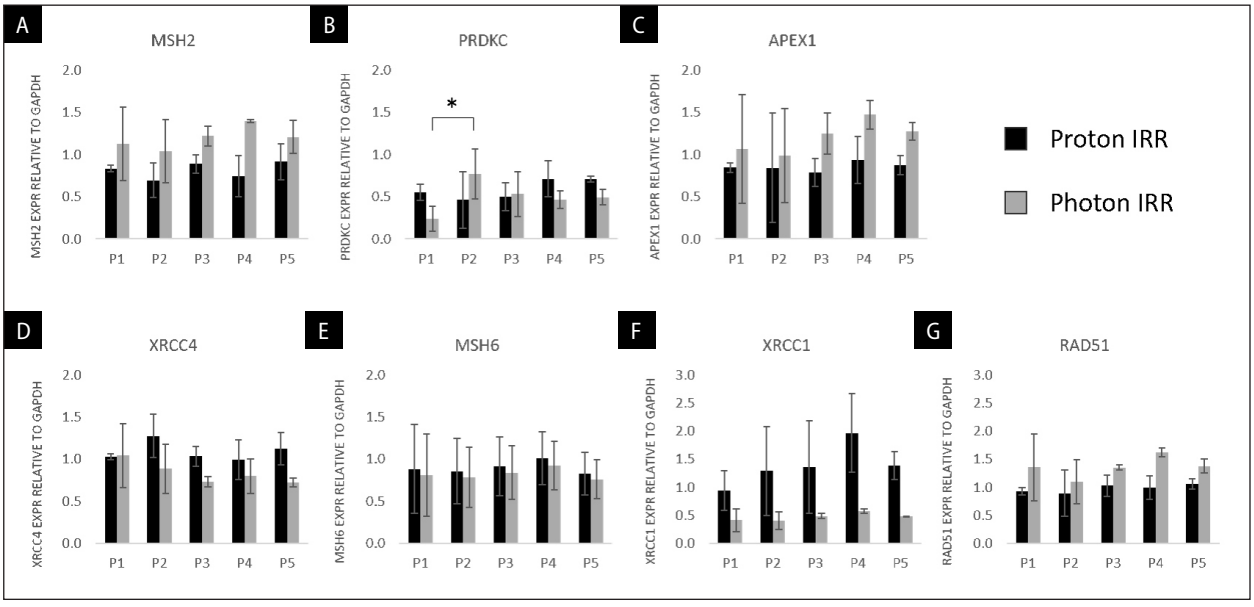

Figure 6. Quantitative polymerase chain reaction (qPCR) analysis expression of genes characteristic for radiobiology response. MDA-MB-231 cells were irradiated using proton (black) and photon (gray) beams in 5 different location along different part of depth-dose curve (P1–P5). The expression of following genes was analyzed: **A.** *MSH2*; **B.** *PRDKC*; **C.** *APEX1*; **D.** *XRCC4*; **E.** *MSH6*; **F.** *XRCC1*; **G.** *RAD51*. The setting of the p-value was *p < 0.05. The error bars represent standard deviation (SD)

radiation. However, a pattern of increased expression of the *PRDKC*, *RAD51* and *XRCC1* genes was observed as the location depth rose. (based on the slope values of the gene expression/dose trendlines). Moreover, the highest value of gene expression was usually observed in the P4 localization considering all genes. Considering photon IRR, the gene response was similar. There was no difference between cells irradiated on various depths along the depth-dose curve, apart from one significant increase ($p = 0.046526$) between P1 and P2 locations in the *PRDKC* gene. The gene expression values were homogenous, analyzing proton and photon beams with some dominant trends depending on the analyzed gene.

Discussion

Tumors are made up of cells that are distributed irregularly and react individually to interactions of ionizing events caused by protons, secondary electrons, or secondary photons. To investigate the radiobiological differences among various parts of the Bragg curve, we used a highly unique irradiation model for the first time. Usually, analyzed effects of cell IRR in SOBP, which consists of superpositions of single Bragg peaks, are not informative enough to determine the results from individual Bragg peaks. That is why we located cells in different positions along the single Bragg peak, irradiating them with the same dose of 5 Gy. We aimed to observe possible heterogenic response induced by ionization through different processes which are more likely to occur at specific areas of the percentage dose depth for a proton beam. The topic of relative biological effectiveness for proton beams is widely researched due to the averaged and assumed RBE value of 1.1 compared to photon beams [16–18]. However, this value can vary depending on many factors; one is the position relative to the Bragg peak, characterized by an increased LET [16]. Therefore, the effect of RBE was not considered in this experiment.

Our findings, including SF after proton and photon IRR, were comparable, except for the location just after the Bragg peak, where SF reached a statistically lower value after exposure to the proton beam. Moreover, a tendency of decreasing SF with increasing depth after proton IRR was observed. One of the first studies investigating the effects along the Bragg peak using proton beams was the research conducted by Bettega et al. [19]. They used 65 MeV proton beams for irradiating SCC25 eye tumor cells. Results of IRR in 5 chosen points in SOBP indicated RBE values reaching 1.1–1.2, whereas at the distal declining edge, values increased to 2. Compared to the applied reference (photon beam), there was no difference in cell survival between various IRRs at the first location (P1) as in our study. Moreover, they showed similar results to ours, including a comparison of the survival curves. The results showed that at the same dose, survival dropped with increasing depth along the depth-dose curve.

The depth distribution of dose for a proton beam is primarily influenced by three factors: the enhanced braking potential of protons as their velocity diminishes, Coulomb scattering of protons when interacting with the nuclei of the medium, and the energetic dispersion of the beam due to the statistical nature of proton ionization and scattering on the nuclei and electrons of the medium. Various nuclear reactions taking place between protons and matter across the depth-dose curve might result in diverse radiobiological reactions, depending on the irradiation's position along the Bragg curve. In our study, as the depth at which MDA-MB-231 cells were irradiated increased, the number of DNA DSBs was higher. The diversities between these effects compared to the results obtained after photon IRR showed not only that protons induce a higher level of γH2AX but also that behind the Bragg peak, there is a probability of inducing more DNA DSBs than in front of or in the Bragg peak. In a recent study, another BC cell line, MCF-7, was irradiated using proton and carbon beams [20]. Radiobiological parameters, such as Bac/Bc ratio and higher subG1 fraction, highlighted that carbon ions were more effective in decreasing cellular proliferation than proton IRR, although no statistical variety was observed in γH2AX foci. Keta et al. [21] investigated the complex relationship between LET and biological response to proton IRR and the conventional photons and high LET carbon ions. Using MCF-7 BC cells, HTB140 melanoma and HTB177 non-small lung cancer cells, they carried out an immunofluorescence based assay to assess the amount of DNA double strand-breaks (DSB) induced by various LET values. As in our study, the γH2AX level raised with the increasing LET at the distal end of SOBP,

although for the highest LET value in the distal fall-off part, the γH2AX level decreased. Moreover, proton IRR was more effective in inducing DSB than photons in most cases. Calugaru et al. [22] analyzed of cell killing and the incidence of DSBs using proton beams. They used two different energy beams, 76 MeV and 201 MeV, for cell IRR. Considering applied photon beams, the number of DNA DSB and clustered lesions was higher after proton IRR. The metastatic potential in MDA-MB-231 cells after proton IRR was analyzed by Lee et al. [23]. They concluded that the proton beam might cause a block of the Akt signaling pathway, limiting cancer development and metastatic spread by suppressing cyclooxygenase 2 (COX-2) and matrix metalloproteinase-9 (MMP-9) expressions.

At the genetic level, we found no indication of differences between BC cells irradiated at various locations. A standard suite of genes related to the DNA damage response was applied and some trends in gene expression were observed, but no direct conclusions can be drawn. Assessing gene expression is challenging because the time factor after IRR is crucial. In the future, it would be necessary to check gene expression at other time points or focus on possible signaling pathways related to the induction of DNA DSBs after proton radiation. A deeper understanding of molecular radiobiological response was proposed by Choi et al. [24] who used 10 BC cell lines to assess RBE results after 230 MeV proton IRR compared to 6 MV X-rays. Cyclin D1 abundance in cells was linked to proton RBE. Downregulation of RB1 by siRNA or a CDK4/6 inhibitor increased proton sensitivity in BC cells but not proton RBE. In contrast, cyclin D1 depletion boosted proton RBE in two TNBC cell lines, MDA-MB-231 and Hs578T. Their findings provide insights into the cyclin D1-CDK4-RB1 pathway as a potential target for proton beam treatment in TNBC.

Conclusion

The cellular response along the Bragg peak is likely to be highly heterogenic as shown by DNA DSB level. The diversities between these effects showed that behind the Bragg peak, there is a probability of inducing more DNA DSBs than in front of the peak or in the Bragg peak. The reaction of cancer cells to proton beam radiation varied significantly in both quantity and quality across the dose build-up and fall-off areas. These results indicate that even with a uniform proton dose within the target, the biological response can be diverse, holding an important indication for clinical practice.

Authors' contributions

M.M., K.G. and M.L. performed the measurements, W.S., T.P., B.S. and J.M. were involved in planning and supervised the work, M.M. processed the experimental data, performed the analysis, drafted the manuscript and designed the figures. L.P. carried out the part of experiments. M.M. and K.G. aided in interpreting the results and worked on the manuscript. All authors discussed the results and commented on the manuscript.

Acknowledgements

The study was supported by the Greater Poland Cancer Centre in Poznan, Poland, and the Skandion Clinic and Rudbeck Laboratory in Uppsala, Sweden.

Competing interest

The authors declare that they have no competing interests.

Funding

This research was funded by the National Science Centre, based on the decision number DEC-2019/35/B/NZ7/04342 (grant number: 2019/35/B/NZ7/04342) and The Swedish Cancer Society (22 2365 Pj).

References

1. Larrson B, Leksell L, Rexed B, et al. The high-energy proton beam as a neurosurgical tool. Nature. 1958; 182(4644): 1222–1223, doi: 10.1038/1821222a0, indexed in Pubmed: 13590280.
2. Musielak M, Suchorska WM, Fundowicz M, et al. Future Perspectives of Proton Therapy in Minimizing the Toxicity of Breast Cancer Radiotherapy. J Pers Med. 2021; 11(5), doi: 10.3390/jpm11050410, indexed in Pubmed: 34068305.
3. Fokas E, Kraft G, An H, et al. Ion beam radiobiology and cancer: time to update ourselves. Biochim Biophys Acta. 2009; 1796(2): 216–229, doi: 10.1016/j.bbcan.2009.07.005, indexed in Pubmed: 19682551.
4. Alaswad M. Locally advanced non-small cell lung cancer: current issues and recent trends. Rep Pract Oncol Radiother. 2023; 28(2): 286–303, doi: 10.5603/RPOR.a2023.0019, indexed in Pubmed: 37456701.

5. Gungor Price GM, Sarigul N. The effect of voxelization in Monte Carlo simulation to validate Bragg peak characteristics for a pencil proton beam. Rep Pract Oncol Radiother. 2023; 28(1): 102–113, doi: 10.5603/RPOR.a2023.0007, indexed in Pubmed: 37122904.
6. Sayan M, Jan I, Vergalasova I, et al. Incidence of clinical lymphedema in breast cancer patients treated with adjuvant proton-based radiotherapy. Rep Pract Oncol Radiother. 2022; 27(3): 474–478, doi: 10.5603/RPOR.a2022.0053, indexed in Pubmed: 36186685.
7. Jia S, Romano F, Cirrone G, et al. Designing a range modulator wheel to spread-out the Bragg peak for a passive proton therapy facility. Nucl Instr Meth Phys Res Sect A. 2016; 806: 101–108, doi: 10.1016/j.nima.2015.10.006.
8. Podgoršak EB. International Atomic Energy Agency, (eds.). Radiation oncology physics: a handbook for teachers and students. International Atomic Energy Agency, Vienna 2005.
9. Nikjoo H, O'Neill P, Wilson WE, et al. Computational Approach for Determining the Spectrum of DNA Damage Induced by Ionizing Radiation. Radiat Res. 2001; 156(5): 577–583, doi: 10.1667/0033-7587(2001)156[0577:cafdts]2.0.co;2, indexed in Pubmed: 11604075.
10. Mohan R, Peeler CR, Guan F, et al. Radiobiological issues in proton therapy. Acta Oncol. 2017; 56(11): 1367–1373, doi: 10.1080/0284186X.2017.1348621, indexed in Pubmed: 28826292.
11. Wang CC, McNamara AL, Shin J, et al. End-of-Range Radiobiological Effect on Rib Fractures in Patients Receiving Proton Therapy for Breast Cancer. Int J Radiat Oncol Biol Phys. 2020; 107(3): 449–454, doi: 10.1016/j.ijrobp.2020.03.012, indexed in Pubmed: 32240774.
12. Ilicic K, Combs SE, Schmid TE. New insights in the relative radiobiological effectiveness of proton irradiation. Radiat Oncol. 2018; 13(1): 6, doi: 10.1186/s13014-018-0954-9, indexed in Pubmed: 29338744.
13. Almond PR, Biggs PJ, Coursey BM, et al. AAPM's TG-51 protocol for clinical reference dosimetry of high-energy photon and electron beams. Med Phys. 1999; 26(9): 1847–1870, doi: 10.1118/1.598691, indexed in Pubmed: 10505874.
14. International Atomic Energy Agency. Absorbed Dose Determination in External Beam Radiotherapy. International Atomic Energy Agency 2000.
15. Sessler A, Wilson E. Engines of Discovery: A Century of Particle Accelerators Revised and Expanded Edition. World Scietific 2014.
16. Lühr A, von Neubeck C, Krause M, et al. Relative biological effectiveness in proton beam therapy - Current knowledge and future challenges. Clin Transl Radiat Oncol. 2018; 9: 35–41, doi: 10.1016/j.ctro.2018.01.006, indexed in Pubmed: 29594249.
17. McMahon SJ. Proton RBE models: commonalities and differences. Phys Med Biol. 2021; 66(4): 04NT02, doi: 10.1088/1361-6560/abda98, indexed in Pubmed: 33429381.
18. Vaniqui A, Vaassen F, Di Perri D, et al. Linear Energy Transfer and Relative Biological Effectiveness Investigation of Various Structures for a Cohort of Proton Patients With Brain Tumors. Adv Radiat Oncol. 2023; 8(2): 101128, doi: 10.1016/j.adro.2022.101128, indexed in Pubmed: 36632089.
19. Bettega D, Calzolari P, Chauvel P, et al. Radiobiological studies on the 65 MeV therapeutic proton beam at Nice using human tumour cells. Int J Radiat Biol. 2000; 76(10): 1297–1303, doi: 10.1080/09553000050151565, indexed in Pubmed: 11057737.
20. Ristic-Fira A, Keta O, Petković V, et al. DNA damage assessment of human breast and lung carcinoma cells irradiated with protons and carbon ions. J Radiat Res Appl Sci. 2020; 13(1): 672–687, doi: 10.1080/16878507.2020.1825035.
21. Keta O, Petković V, Cirrone P, et al. DNA double-strand breaks in cancer cells as a function of proton linear energy transfer and its variation in time. Int J Radiat Biol. 2021; 97(9): 1229–1240, doi: 10.1080/09553002.2021.1948140, indexed in Pubmed: 34187289.
22. Calugaru V, Nauraye C, Noël G, et al. Radiobiological characterization of two therapeutic proton beams with different initial energy spectra used at the Institut Curie Proton Therapy Center in Orsay. Int J Radiat Oncol Biol Phys. 2011; 81(4): 1136–1143, doi: 10.1016/j.ijrobp.2010.09.003, indexed in Pubmed: 21075549.
23. Lee KS, Lee DH, Chun SY, et al. Metastatic potential in MDA-MB-231 human breast cancer cells is inhibited by proton beam irradiation via the Akt/nuclear factor-κB signaling pathway. Mol Med Rep. 2014; 10(2): 1007–1012, doi: 10.3892/mmr.2014.2259, indexed in Pubmed: 24859472.
24. Choi C, Park S, Cho WK, et al. Cyclin D1 is Associated with Radiosensitivity of Triple-Negative Breast Cancer Cells to Proton Beam Irradiation. Int J Mol Sci. 2019; 20(19), doi: 10.3390/ijms20194943, indexed in Pubmed: 31591311.